

# Hadron-Quark Phase Transitions in Hyperon Stars

N. Yasutake,<sup>1</sup> G.F. Burgio,<sup>2</sup> and H.-J. Schulze<sup>2</sup>

<sup>1</sup> *Division of Theoretical Astronomy, National Astronomical Observatory of Japan,  
2-21-1 Osawa, Mitaka, Tokyo 181-8588, Japan*

<sup>2</sup> *INFN, Sezione di Catania, Via Santa Sofia 64, I-95123 Catania, Italy*

We compare the Gibbs and Maxwell constructions for the hadron-quark phase transition in neutron and protoneutron stars, including interacting hyperons in the confined phase. We find that the hyperon populations are suppressed and that neutrino trapping shifts the onset of the phase transition. The effects on the (proto)neutron star maximum mass are explored.

PACS numbers: 26.60.Kp, 26.60.-c, 26.50.+x

## I. INTRODUCTION

Some recent lattice QCD calculations have improved our knowledge on the nature of the nucleon-hyperon (NY) and hyperon-hyperon (YY) interactions [1]. Moreover, an intense experimental activity aimed at exploring hypernuclei has started at the J-PARC facility, which will hopefully clarify in the near future some unresolved questions on the hyperon interactions. This will help to improve the theoretical modeling of neutron star (NS) interiors, where hyperons are predicted to be present in large fractions, and many aspects of the equation of state (EOS) could be clarified.

There are essentially two microscopic approaches to derive the properties and the EOS of dense matter starting from the bare baryon-baryon interactions, namely the Brueckner-Hartree-Fock (BHF) theory [2] and the variational method [3]. Including the hyperon degrees of freedom, the EOS becomes very soft, and in the BHF approach the maximum mass for a NS lies below currently observed values of about  $1.7 M_{\odot}$  [4]. To overcome this problem, some possibilities have been suggested: i) The repulsive effects of three-body forces (TBF) among nucleons and hyperons, which may stiffen the EOS [5]; ii) Additional repulsion coming from hyperon-hyperon interactions (but no experimental data are available so far); iii) The hadron-quark phase transition [6, 7], which could lead to a partial suppression of the hyperon population, thus stiffening the EOS. This conclusion needs to be further explored, since at present there are many uncertainties regarding the quark matter EOS.

The scope of this work is to present results on the composition and structure of neutron and protoneutron stars (PNS), which are produced in the aftermath of successful supernova (SN) explosions of very massive stars ( $M \gtrsim 8 M_{\odot}$ ). These objects can reach temperatures of the order of 30–40 MeV in their interiors, and are characterized by a temporary neutrino trapping with a conserved lepton fraction  $Y_e \approx 0.4$  [8, 9], lasting some seconds. Both thermal effects and neutrino trapping may result in observable consequences of the neutrino signature from a supernova, and may also play an important role in determining whether a SN ultimately produces a cold NS or a black hole. In this paper, we focus on the hadron-quark phase transition, with the explicit inclusion of interacting hyperons in the confined phase. For hadronic matter we adopt the BHF microscopic EOS extended to finite temperature, and use the MIT bag model in the quark phase.

This paper is organized as follows. In Section II we illustrate the Brueckner-Bethe-

Goldstone (BBG) many-body theory including hyperons at finite temperature. Sections III and IV briefly review the MIT bag model and the treatment of the hadron-quark mixed phase, respectively. In Section V we discuss our results regarding the structure of NSs and PNSs, in particular their maximum mass. Final conclusions are drawn in Section VI.

## II. HADRON PHASE: THE BBG THEORY AT FINITE TEMPERATURE

In the recent years, the BBG perturbative theory [2] has been extended in a fully microscopic way to the finite-temperature case [10], according to the formalism developed by Bloch and De Dominicis [11]. In this approach the essential ingredient is the two-body scattering matrix  $G$ , which in the finite-temperature extension is determined by solving numerically the Bethe-Goldstone equation, written in operatorial form as

$$G_{ab}[W] = V_{ab} + \sum_c \sum_{p,p'} V_{ac} |pp'\rangle \frac{Q_c}{W - E_c + i\varepsilon} \langle pp' | G_{cb}[W], \quad (1)$$

where the indices  $a, b, c$  indicate pairs of baryons and the Pauli operator  $Q$  and energy  $E$  determine the propagation of intermediate baryon pairs. In a given baryon-baryon channel  $c = (12)$  one has

$$Q_{(12)} = [1 - n_1(k_1)][1 - n_2(k_2)], \quad (2)$$

$$E_{(12)} = m_1 + m_2 + e_1(k_1) + e_2(k_2) \quad (3)$$

with the single-particle energy  $e_i(k) = k^2/2m_i + U_i(k)$ , the Fermi distribution  $n_i(k) = (e^{[e_i(k) - \bar{\mu}_i]/T} + 1)^{-1}$ , the starting energy  $W$ , and the two-body interaction (bare potential)  $V$  as fundamental input. The various single-particle potentials within the continuous choice are given by

$$U_1(k_1) = \text{Re} \sum_{2=n,p,\Lambda,\Sigma} \sum_{k_2} n(k_2) \langle k_1 k_2 | G_{(12)(12)}[E_{(12)}] | k_1 k_2 \rangle_A, \quad (4)$$

where  $k_i$  generally denote momentum and spin.

We choose the Argonne  $V_{18}$  nucleon-nucleon potential [12] as two-body interaction  $V$ , supplemented by TBF among nucleons, in order to reproduce correctly the nuclear matter saturation point  $\rho_0 \approx 0.17 \text{ fm}^{-3}$ ,  $E/A \approx -16 \text{ MeV}$ . As TBF, we use the phenomenological Urbana model [13], which is actually reduced to a density-dependent two-body force by averaging over the position of the third particle [10, 14].

Recently, the BHF approach has been extended by including consistently interacting hyperons at finite temperature [15]. In the hyperonic sector we employed the Nijmegen soft-core NY potentials NSC89 [16], fitted to the available experimental NY scattering data. Since at zero temperature only  $\Lambda$  and  $\Sigma^-$  hyperons appear in the neutron star matter up to very large densities [17], we restrict also the present study to these two hyperon species. Therefore, for fixed partial densities  $\rho_i = \sum_k n_i(k)$ , ( $i = n, p, \Lambda, \Sigma^-$ ) and temperature  $T$ , we solve self-consistently Eqs. (1) and (4) and calculate then the free energy density, which has the following simplified expression

$$f = \sum_i \left[ \sum_k n_i(k) \left( \frac{k^2}{2m_i} + \frac{1}{2} U_i(k) \right) - T s_i \right], \quad (5)$$

where

$$s_i = - \sum_k \left( n_i(k) \ln n_i(k) + [1 - n_i(k)] \ln[1 - n_i(k)] \right) \quad (6)$$

is the entropy density for component  $i$  treated as a free gas with spectrum  $e_i(k)$ . All thermodynamic quantities of interest can then be computed from the free energy density, Eq. (5); namely, the chemical potentials  $\mu_i$ , pressure  $p$ , entropy density  $s$ , and internal energy density  $\varepsilon$  read as

$$\mu_i = \frac{\partial f}{\partial \rho_i}, \quad (7)$$

$$p = \rho^2 \frac{\partial(f/\rho)}{\partial \rho} = \sum_i \mu_i \rho_i - f, \quad (8)$$

$$s = - \frac{\partial f}{\partial T}, \quad (9)$$

$$\varepsilon = f + Ts, \quad (10)$$

where  $\rho = \sum_i \rho_i$  is the baryon number density.

However, due to the large number of degrees of freedom (4 partial densities + temperature), it is necessary to introduce some approximations in order to speed up the calculations. We adopt the so-called Frozen Correlations Approximation (FCA), assuming the correlations at  $T \neq 0$  to be essentially the same as at  $T = 0$ . This means that the single-particle potential  $U_i(k)$  for the component  $i$  can be approximated by the one calculated at  $T = 0$ . Furthermore, we fit the numerical results by a sufficiently accurate analytical parametrization. We find that the following functional form provides an excellent parametrization of the numerical data for the free energy density in the required ranges of nucleon density ( $0.1 \text{ fm}^{-3} \lesssim \rho_N \lesssim 0.8 \text{ fm}^{-3}$ ), hyperon fractions ( $0 \leq \rho_\Lambda/\rho_N \leq 0.9$ ,  $0 \leq \rho_\Sigma/\rho_N \leq 0.5$ ), and temperature ( $0 \text{ MeV} \leq T \leq 50 \text{ MeV}$ ):

$$\begin{aligned} f(\rho_n, \rho_p, \rho_\Lambda, \rho_\Sigma, T) &= F_N \rho_N \\ &+ (F_\Lambda + F_{\Lambda\Lambda} + F_{\Lambda\Sigma}) \rho_\Lambda + \frac{C}{2m_\Lambda M_\Lambda} \rho_\Lambda^{5/3} \\ &+ (F_\Sigma + F_{\Sigma\Sigma} + F_{\Sigma\Lambda}) \rho_\Sigma + \frac{C}{2m_\Sigma M_\Sigma} \rho_\Sigma^{5/3} \end{aligned} \quad (11)$$

with the parametrizations at zero temperature:

$$F_N = (1 - \beta) (a_0 \rho_N + b_0 \rho_N^{c_0}) + \beta (a_1 \rho_N + b_1 \rho_N^{c_1}), \quad (12)$$

$$F_Y = (a_Y^0 + a_Y^1 x + a_Y^2 x^2) \rho_N + (b_Y^0 + b_Y^1 x + b_Y^2 x^2) \rho_N^{c_Y}, \quad (13)$$

$$F_{YY'} = a_{YY'} \rho_N^{c_{YY'}} \rho_{Y'}^{d_{YY'}}, \quad (14)$$

$$M_Y = 1 + (c_Y^0 + c_Y^1 x) \rho_N, \quad (15)$$

where  $\rho_N = \rho_n + \rho_p$ ;  $x = \rho_p/\rho_N$ ;  $\beta = (1-2x)^2$ ;  $C = (3/5)(3\pi^2)^{2/3} \approx 5.742$ ; and  $Y, Y' = \Lambda, \Sigma^-$ . At finite temperature the expressions are extended as follows:

$$\begin{aligned} F_N &= F_N(T=0) \\ &+ \left[ \tilde{a}_0 t^2 \rho_N + (\tilde{d}_0 t^2 + \tilde{e}_0 t^3) \ln(\rho_N) + \tilde{f}_0 t^2 / \rho_N \right] (1 - \beta) \end{aligned}$$

TABLE I: Fit parameters for the free energy density, Eqs. (11-18).

$a_0, b_0, c_0, a_1, b_1, c_1$	-286.6	397.2	1.39	88.1	207.7	2.50
$a_\Lambda^0, a_\Lambda^1, a_\Lambda^2, b_\Lambda^0, b_\Lambda^1, b_\Lambda^2, c_\Lambda$	-403	688	-943	659	-1273	1761 1.72
$a_\Sigma^0, a_\Sigma^1, a_\Sigma^2, b_\Sigma^0, b_\Sigma^1, b_\Sigma^2, c_\Sigma$	-114	0	0	291	0	0 1.63
$a_{\Lambda\Lambda}, c_{\Lambda\Lambda}, d_{\Lambda\Lambda}$	136	0.51	0.93			
$a_{\Lambda\Sigma}, c_{\Lambda\Sigma}, d_{\Lambda\Sigma}$	0	0	0			
$a_{\Sigma\Sigma}, c_{\Sigma\Sigma}, d_{\Sigma\Sigma}$	0	0	0			
$a_{\Sigma\Lambda}, c_{\Sigma\Lambda}, d_{\Sigma\Lambda}$	89	0.33	0.81			
$c_\Lambda^0, c_\Lambda^1, c_\Sigma^0, c_\Sigma^1$	0.22	-0.38	-0.59	-0.22		
$\tilde{a}_0, \tilde{d}_0, \tilde{e}_0, \tilde{f}_0$	-202.0	396.9	-190.6	35.2		
$\tilde{a}_1, \tilde{d}_1, \tilde{e}_1, \tilde{f}_1$	-138.0	308.4	-109.3	31.2		
$\tilde{d}_\Lambda, \tilde{e}_\Lambda, \tilde{f}_\Lambda, \tilde{g}_\Lambda, \tilde{b}_\Lambda, \tilde{c}_\Lambda$	92.3	29.3	39.4	152.3	4.78	3.95
$\tilde{d}_\Sigma, \tilde{e}_\Sigma, \tilde{f}_\Sigma, \tilde{g}_\Sigma, \tilde{b}_\Sigma, \tilde{c}_\Sigma$	89.2	61.0	63.6	186.8	1.13	3.30

$$+ \left[ \tilde{a}_1 t^2 \rho_N + (\tilde{d}_1 t^2 + \tilde{e}_1 t^3) \ln(\rho_N) + \tilde{f}_1 t^2 / \rho_N \right] \beta, \quad (16)$$

$$F_Y = F_Y(T = 0)$$

$$+ (\tilde{d}_Y t^2 + \tilde{e}_Y t^3) \ln(\rho_N) + \tilde{f}_Y t^2 / \rho_N + \tilde{g}_Y t^2 \ln(\rho_Y), \quad (17)$$

$$M_Y = M_Y(T = 0) + \tilde{b}_Y t^2 \rho_N^{\tilde{c}_Y}, \quad (18)$$

where  $t = T/(100 \text{ MeV})$  and  $f$  and  $\rho_i$  are given in  $\text{MeV fm}^{-3}$  and  $\text{fm}^{-3}$ , respectively, (and  $m_{\Lambda, \Sigma}$  in  $\text{MeV}^{-1} \text{fm}^{-2}$ ).

Technically, these parametrizations were obtained by performing about  $10^3$  BHF calculations at zero temperature in the  $(\rho_n, \rho_p, \rho_\Lambda, \rho_\Sigma)$ -space and then using the FCA to generate finite-temperature results, increasing by about one order of magnitude the number of “data” points  $f(\rho_n, \rho_p, \rho_\Lambda, \rho_\Sigma, T)$ . The optimal values of the fit parameters, listed in Table I, were then determined hierarchically for cold nuclear matter, cold hypernuclear matter, hot nuclear matter, hot hypernuclear matter, so that the fits are optimized also in the more constrained cases [15].

### III. QUARK PHASE: THE MIT BAG MODEL

For the quark phase, we adopt the MIT bag model involving  $u$ ,  $d$  and  $s$  quarks [6, 7, 18]. Probably, this model is too simple to describe quark matter in a realistic way, and we plan to adopt more sophisticated models in the future [19–21]. We assume massless  $u$  and  $d$  quarks,  $s$  quarks with a current mass of  $m_s = 150 \text{ MeV}$ , and a density-dependent (but temperature-independent) bag constant,

$$B(\rho) = B_\infty + (B_0 - B_\infty) \exp \left[ -\beta \left( \frac{\rho}{\rho_0} \right)^2 \right] \quad (19)$$

with  $B_\infty = 50 \text{ MeV fm}^{-3}$ ,  $B_0 = 400 \text{ MeV fm}^{-3}$ , and  $\beta = 0.17$ .

This approach has been proposed in Ref. [6] on the basis of experimental results on the formation of a quark-gluon plasma obtained at the CERN SPS. The above choice of the parameters allows the symmetric nuclear matter to be in the pure hadronic phase at low densities, and in the quark phase at large densities, while the transition density is taken as

a parameter. Several possible choices of the parameters have been explored in [6], and all give a NS maximum mass in a relatively narrow interval,  $1.4 M_\odot \lesssim M_{\text{max}} \lesssim 1.7 M_\odot$ . For a more extensive discussion of this topic, the reader is referred to [18], where details regarding the MIT bag model at finite temperature are also given, which will not be repeated here.

#### IV. MIXED PHASE

With this parametrization of the density dependence of  $B$  we now consider the hadron-quark phase transition in (proto)neutron stars. We calculate the EOS of a conventional neutron star as composed of a chemically equilibrated and charge-neutral mixture of nucleons, hyperons, and leptons. We do not take into account anti-particles and muons in this paper, since their effects on the EOS are very small.

We compare numerical results obtained using the Maxwell and the Gibbs constructions for the phase transition. We remind that in the Maxwell construction both phases are charge neutral and the conditions of mechanical and chemical equilibrium determine a coexistence phase, which is described by a constant pressure plateau typical of a liquid-vapor phase transition. On the other hand, in the Gibbs construction [22] both the hadron and the quark phase are allowed to be separately charged, still preserving the total charge neutrality. This implies that neutron star matter can be treated as a two-component system, and therefore can be parametrized by two chemical potentials. Usually one chooses the pair  $(\mu_e, \mu_n)$ , i.e., electron and baryon chemical potential. The pressure is the same in the two phases to ensure mechanical stability, while the chemical potentials of the different species are related to each other, satisfying chemical and beta stability. As a consequence, the pressure turns out to be a monotonically increasing function of the density, at variance with the Maxwell construction. We note that our Gibbs treatment is the zero surface tension limit in the calculations including finite-size effects [23, 24].

The Gibbs conditions for chemical and mechanical equilibrium at finite temperature between both phases read

$$\mu_u + \mu_e - \mu_{\nu_e} = \mu_d = \mu_s, \quad (20)$$

$$\mu_p + \mu_e - \mu_{\nu_e} = \mu_n = \mu_\Lambda = \mu_u + 2\mu_d, \quad (21)$$

$$\mu_{\Sigma^-} + \mu_p = 2\mu_n, \quad (22)$$

$$p_H(\mu_e, \mu_n, T) = p_Q(\mu_e, \mu_n, T) = p_M. \quad (23)$$

From these equations one can calculate the equilibrium chemical potentials of the mixed phase corresponding to the intersection of the two surfaces representing the hadron and the quark phase, which allows one to calculate the charge densities  $\rho_c^H$  and  $\rho_c^Q$  and therefore the volume fraction  $\chi$  occupied by quark matter in the mixed phase, i.e.,

$$\chi\rho_c^Q + (1 - \chi)\rho_c^H = 0. \quad (24)$$

From this, the energy density  $\epsilon_M$  and the baryon density  $\rho_M$  of the mixed phase can be determined as

$$\epsilon_M = \chi\epsilon_Q + (1 - \chi)\epsilon_H, \quad (25)$$

$$\rho_M = \chi\rho_Q + (1 - \chi)\rho_H. \quad (26)$$

## V. RESULTS AND DISCUSSION

In Fig. 1 we show the particle fractions obtained by applying the Gibbs construction to NS matter ( $T = 0$  MeV and  $x_{\nu_e} = 0$ , upper panel), and to SN matter ( $T = 40$  MeV and  $Y_e = 0.4$ , lower panel). We observe that hyperons do not appear at all in the NS mixed phase, because the onset for the hadron-quark phase transition takes place at densities below the hyperon onset. In SN matter, thermal hyperons appear already at low density, but they are negligible. Hence, we conclude that the quarks suppress the hyperons in both cases.

The resulting EOS  $p(\rho_B)$  is displayed in Fig. 2, where the upper (lower) panel displays the calculations performed for NS (SN) matter. The pure hadronic (quark) phase is represented by the solid red (dashed green) curve, whereas the mixed phase is indicated by the blue (pink) broken line if the Gibbs (Maxwell) conditions are applied. We observe that the Gibbs mixed phase spans over a wide range of density, around  $0.20$ – $0.74$   $\text{fm}^{-3}$  for NS matter, and slightly less for SN matter,  $0.29$ – $0.71$   $\text{fm}^{-3}$ , because finite temperature counteracts the coexistence of phases, see Ref. [24]. Compared to the EOS with the Gibbs construction, the density jump obtained with the Maxwell construction appears over a narrower density range in NS matter, whereas for SN matter the transition takes place at reduced pressure and over a wider density range, which is mainly due to the trapping condition, as explained in Ref. [18].

The EOSs discussed above are the fundamental input for calculating the stable configurations of compact stars. For that, we use the well-known hydrostatic equilibrium equations of Tolman, Oppenheimer, and Volkov [25]. For completeness, as in [26], we have attached the Shen EOS [27] in the low-density regime ( $\rho < 0.1$   $\text{fm}^{-3}$ ), since below this threshold clusterization sets in and nuclear matter becomes inhomogeneous.

In Fig. 3 we display the gravitational mass (in units of the solar mass,  $M_\odot = 1.99 \times 10^{33} g$ ) as function of the central baryon number density  $\rho_{B,C}$ . The upper (lower) panel shows results for NS (SN) matter, and the blue (pink) broken lines represent the calculations performed with the Gibbs (Maxwell) construction. For comparison, we also display the stable configurations in the pure hadronic phase (solid red line).

We find that in NSs the pure hadronic EOS with hyperons gives rise to a maximum mass smaller than the canonical value, i.e.  $1.44 M_\odot$ , whereas the hadron-quark phase transition allows to reach maximum masses slightly above  $1.5 M_\odot$  (the difference between Gibbs and Maxwell case being very small). This increase is due to the fact that the hyperon populations are suppressed by the existence of quarks, as shown in Fig. 1.

On the contrary, in the SN case all maximum masses are larger than  $1.44 M_\odot$ , but here the phase transition lowers the maximum mass with respect to the purely hadronic matter, because trapping reduces the hyperon concentrations in the latter case compared to NS matter. Also, we observe that the value of the maximum mass with the Gibbs condition is slightly higher than the one with the Maxwell construction, which is due to the overall higher pressure of the matter in the former case, see Fig. 2.

We also find that the stars with a mass close to the maximum one have quark cores.

## VI. CONCLUSIONS

We have studied the quark-hadron mixed phase in cold neutron stars and hot neutrino-trapped protoneutron stars containing also hyperons, and compared explicitly the Maxwell and the Gibbs phase transition constructions.

We find that pure quark matter appears in the cores of compact stars in any situation and that the hyperon fractions are nearly completely suppressed by the appearance of quarks. Due to this reason the maximum NS mass is increased by the presence of quark matter. However, the simple MIT bag model used here is not capable to reach currently observed NS masses of about  $1.7 M_{\odot}$  [4], and it will be an important task for the future to implement more sophisticated quark models.

Apart from this challenge, in this paper we did not consider finite-size effects in the mixed phase. In particular, it will be interesting to check the influence of trapped neutrinos on the pasta structures in future works.

### Acknowledgments

We are grateful to M. Baldo, T. Maruyama, and T. Tatsumi for their warm hospitality and fruitful discussions. This study was supported in part by the Grants-in-Aid for the Scientific Research from the Ministry of Education, Science and Culture of Japan (No. 21105512). We also acknowledge the support of COMPSTAR, a research and training program of the European Science Foundation.

- 
- [1] H. Nemura, N. Ishii, S. Aoki, and T. Hatsuda, *Phys. Lett.* **B673**, 2 (2009).
  - [2] M. Baldo, *Nuclear Methods and the Nuclear Equation of State* (World Scientific, Singapore, 1999).
  - [3] A. Akmal, V.R. Pandharipande, and D.G. Ravenhall, *Phys. Rev.* **C58**, 1804 (1998).
  - [4] J.M. Lattimer and M. Prakash, *Phys. Rep.* **442**, 109 (2007).
  - [5] S. Nishizaki, Y. Yamamoto, and T. Takatsuka, *Prog. Theor. Phys.* **108**, 703 (2002).
  - [6] G.F. Burgio, M. Baldo, P.K. Sahu, and H.-J. Schulze, *Phys. Rev.* **C66**, 025802 (2002).
  - [7] C. Maieron, M. Baldo, G. F. Burgio, and H.-J. Schulze, *Phys. Rev.* **D70**, 043010 (2004).
  - [8] A. Burrows and J.M. Lattimer, *Ap. J.* **307**, 178 (1986).
  - [9] J.A. Pons, S. Reddy, M. Prakash, J.M. Lattimer, and J.A. Miralles, *Ap. J.* **513**, 780 (1999).
  - [10] M. Baldo and L.S. Ferreira, *Phys. Rev.* **C59**, 682 (1999).
  - [11] C. Bloch and C. De Dominicis, *Nucl. Phys.* **7**, 459 (1958); **10**, 181,509 (1959).
  - [12] R.B. Wiringa, V.G.J. Stoks, and R. Schiavilla, *Phys. Rev.* **C51**, 38 (1995).
  - [13] J. Carlson, V.R. Pandharipande, and R.B. Wiringa, *Nucl. Phys.* **A401**, 59 (1983); R. Schiavilla, V.R. Pandharipande, and R.B. Wiringa, *Nucl. Phys.* **A449**, 219 (1986).
  - [14] M. Baldo, I. Bombaci, and G.F. Burgio, *Astron. Astrophys.* **328**, 274 (1997).
  - [15] G.F. Burgio, H.-J. Schulze, and A. Li, submitted to *Phys. Rev. C*.
  - [16] P.M.M. Maessen, Th.A. Rijken, and J.J. de Swart, *Phys. Rev.* **C40**, 2226 (1989).
  - [17] M. Baldo, G.F. Burgio, and H.-J. Schulze, *Phys. Rev.* **C58**, 3688 (1998); **C61**, 055801 (2000); H.-J. Schulze, A. Polls, A. Ramos, and I. Vidaña, *Phys. Rev.* **C73**, 058801 (2006).
  - [18] O.E. Nicotra, M. Baldo, G.F. Burgio, and H.-J. Schulze, *Astron. Astrophys.* **451**, 213 (2006); *Phys. Rev.* **D74**, 123001 (2006).
  - [19] M. Baldo, G.F. Burgio, P. Castorina, S. Plumari, and D. Zappalà, *Phys. Rev.* **C75**, 035804 (2007).
  - [20] H. Chen, W. Yuan, L. Chang, Y.-X. Liu, T. Klähn, and C. D. Roberts, *Phys. Rev.* **D78**, 116015 (2009).

- [21] N. Yasutake and K. Kashiwa, Phys. Rev. **D79**, 043012 (2009).
- [22] N.K. Glendenning, *Compact Stars, Nuclear Physics, Particle Physics, and General Relativity*, 2nd ed. (Springer, New York, 2000).
- [23] T. Maruyama, S. Chiba, H.-J. Schulze, and T. Tatsumi, Phys. Rev. **D76**, 123015 (2007).
- [24] N. Yasutake, T. Maruyama, and T. Tatsumi, Phys. Rev. **D80**, 123009 (2009).
- [25] S.L. Shapiro and S.A. Teukolsky, *Black Holes, White Dwarfs, and Neutron Stars*, (John Wiley & Sons, New York, 1983).
- [26] G.F. Burgio and H.-J. Schulze, Astron. Astrophys. **518**, A17 (2010).
- [27] H. Shen, H. Toki, K. Oyamatsu, and K. Sumiyoshi, Nucl. Phys. **A637**, 435 (1998).

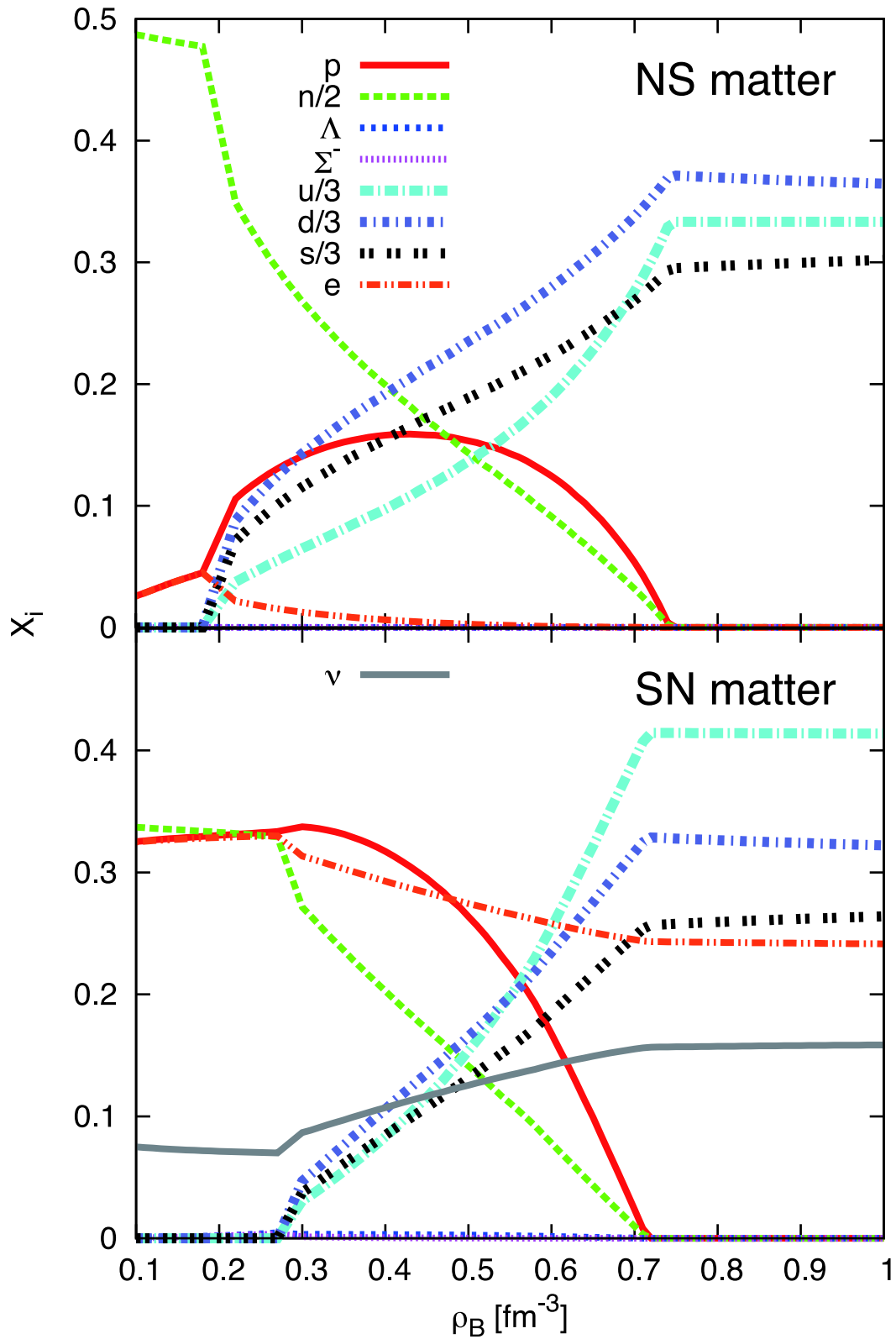


FIG. 1: Particle fractions  $x_i = \rho_i/\rho_B$  as a function of the baryon density  $\rho_B$  for NS (upper panel) and SN matter (lower panel). The mixed phase is calculated by the Gibbs conditions.

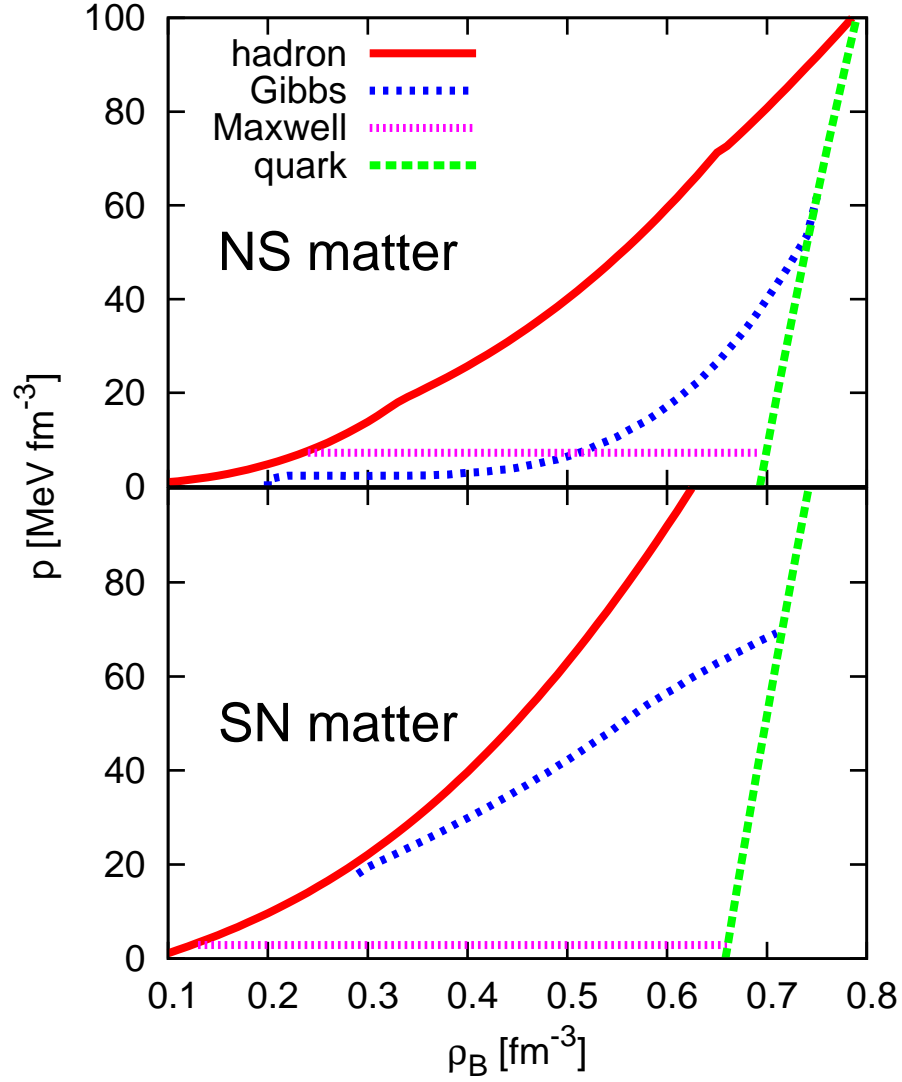


FIG. 2: Pressure as a function of the baryon density for NS (upper panel) and SN matter (lower panel). The red (green) line displays the calculations for purely hadronic (quark) matter. The blue (pink) curve is the coexistence region when the Gibbs (Maxwell) construction is performed.

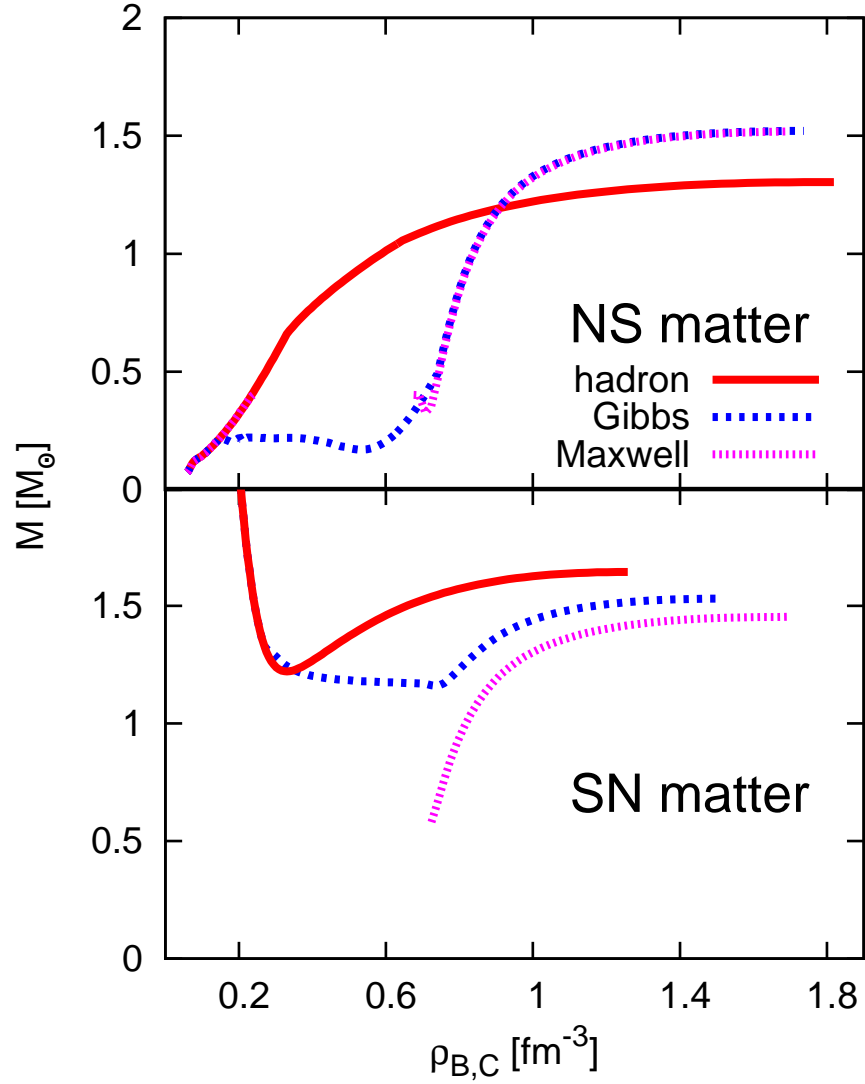


FIG. 3: Gravitational mass (in units of the solar mass) as a function of the central baryon density  $\rho_{B,c}$  for NS (upper panel) and SN (lower panel) matter. The purely hadronic configurations are represented by broken blue lines, whereas the red (green) lines represent the configurations of hybrid stars obtained applying the Gibbs (Maxwell) construction.